Measurement of branching fraction of $D_s^{*+} \to D_s^+\pi^0$ relative to $D_s^{*+} \to D_s^+\gamma$

M. Ablikim[1], M. N. Achasov[11,b], P. Adlarson[70], M. Albrecht[4], R. Aliberti[31], A. Amoroso[69A,69C], M. R. An[35], Q. An[66,53], X. H. Bai[61], Y. Bai[52], O. Bakina[32], R. Baldini Ferroli[26A], I. Balossino[27A], Y. Ban[42,g], V. Batozskaya[1,40], D. Becker[31], K. Begzsuren[29], N. Berger[31], M. Bertani[26A], D. Bettoni[27A], F. Bianchi[69A,69C], J. Bloms[63], A. Bortone[69A,69C], I. Boyko[32], R. A. Briere[5], A. Brueggemann[63], H. Cai[71], X. Cai[1,53], A. Calcaterra[26A], G. F. Cao[1,58], N. Cao[1,58], S. A. Cetin[57A], J. F. Chang[1,53], W. L. Chang[1,58], G. Chelkov[32,a], C. Chen[39], Chao Chen[50], G. Chen[1], H. S. Chen[1,58], M. L. Chen[1,53], S. J. Chen[38], S. M. Chen[56], T. Chen[1], X. R. Chen[28,58], X. T. Chen[1], Y. B. Chen[1,53], Z. J. Chen[23,h], W. S. Cheng[69C], S. K. Choi [50], X. Chu[39], G. Cibinetto[27A], F. Cossio[69C], J. J. Cui[45], H. L. Dai[1,53], J. P. Dai[73], A. Dbeyssi[17], R. E. de Boer[4], D. Dedovich[32], Z. Y. Deng[1], A. Denig[31], I. Denysenko[32], M. Destefanis[69A,69C], F. De Mori[69A,69C], Y. Ding[36], J. Dong[1,53], L. Y. Dong[1,58], M. Y. Dong[1,53,58], X. Dong[71], S. X. Du[75], P. Egorov[32,a], Y. L. Fan[71], J. Fang[1,53], S. S. Fang[1,58], W. X. Fang[1], Y. Fang[1], R. Farinelli[27A], L. Fava[69B,69C], F. Feldbauer[4], G. Felici[26A], C. Q. Feng[66,53], J. H. Feng[54], K Fischer[64], M. Fritsch[4], C. Fritzsch[63], C. D. Fu[1], H. Gao[58], Y. N. Gao[42,g], Yang Gao[66,53], S. Garbolino[69C], I. Garzia[27A,27B], P. T. Ge[71], Z. W. Ge[38], C. Geng[54], E. M. Gersabeck[62], A Gilman[64], K. Goetzen[12], L. Gong[36], W. X. Gong[1,53], W. Gradl[31], M. Greco[69A,69C], L. M. Gu[38], M. H. Gu[1,53], Y. T. Gu[14], C. Y Guan[1,58], A. Q. Guo[28,58], L. B. Guo[37], R. P. Guo[44], Y. P. Guo[10,f], A. Guskov[32,a], T. T. Han[45], W. Y. Han[35], X. Q. Hao[18], F. A. Harris[60], K. K. He[50], K. L. He[1,58], F. H. Heinsius[4], C. H. Heinz[31], Y. K. Heng[1,53,58], C. Herold[55], G. Y. Hou[1,58], Y. R. Hou[58], Z. L. Hou[1], H. M. Hu[1,58], J. F. Hu[51,i], T. Hu[1,53,58], Y. Hu[1], G. S. Huang[66,53], K. X. Huang[54], L. Q. Huang[28,58], X. T. Huang[45], Y. P. Huang[1], Z. Huang[42,g], T. Hussain[68], N Hüsken[25,31], W. Imoehl[25], M. Irshad[66,53], J. Jackson[25], S. Jaeger[4], S. Janchiv[29], E. Jang[50], J. H. Jeong[50], Q. Ji[1], Q. P. Ji[18], X. B. Ji[1,58], X. L. Ji[1,53], Y. Y. Ji[45], Z. K. Jia[66,53], H. B. Jiang[45], S. S. Jiang[35], X. S. Jiang[1,53,58], Y. Jiang[58], J. B. Jiao[45], Z. Jiao[21], S. Jin[38], Y. Jin[61], M. Q. Jing[1,58], T. Johansson[70], N. Kalantar-Nayestanaki[59], X. S. Kang[36], R. Kappert[59], M. Kavatsyuk[59], B. C. Ke[75], I. K. Keshk[4], A. Khoukaz[63], R. Kiuchi[1], R. Kliemt[12], L. Koch[33], O. B. Kolcu[57A], B. Kopf[4], M. Kuemmel[4], M. Kuessner[4], A. Kupsc[40,70], W. Kühn[33], J. J. Lane[62], J. S. Lange[33], P. Larin[17], A. Lavania[24], L. Lavezzi[69A,69C], Z. H. Lei[66,53], H. Leithoff[31], M. Lellmann[31], T. Lenz[31], C. Li[39], C. Li[43], C. H. Li[35], Cheng Li[66,53], D. M. Li[75], F. Li[1,53], G. Li[1], H. Li[47], H. Li[66,53], H. B. Li[1,58], H. J. Li[18], H. N. Li[51,i], J. Q. Li[4], J. S. Li[54], J. W. Li[45], Ke Li[1], L. J Li[1], L. K. Li[1], Lei Li[3], M. H. Li[39], P. R. Li[34,j,k], S. X. Li[10], S. Y. Li[56], T. Li[45], W. D. Li[1,58], W. G. Li[1], X. H. Li[66,53], X. L. Li[45], Xiaoyu Li[1,58], Y. G. Li[42,g], Z. X. Li[14], H. Liang[1,58], H. Liang[30], H. Liang[66,53], Y. F. Liang[49], Y. T. Liang[28,58], G. R. Liao[13], L. Z. Liao[45], J. Libby[24], A. Limphirat[55], C. X. Lin[54], D. X. Lin[28,58], T. Lin[1], B. J. Liu[1], C. X. Liu[1], D. Liu[17,66], F. H. Liu[48], Fang Liu[1], Feng Liu[6], G. M. Liu[51,i], H. Liu[34,j,k], H. B. Liu[14], H. M. Liu[1,58], Huanhuan Liu[1], Huihui Liu[19], J. B. Liu[66,53], J. L. Liu[67], J. Y. Liu[1,58], K. Liu[1], K. Y. Liu[36], Ke Liu[20], L. Liu[66,53], Lu Liu[39], M. H. Liu[10,f], P. L. Liu[1], Q. Liu[58], S. B. Liu[66,53], T. Liu[10,f], W. K. Liu[39], W. M. Liu[66,53], X. Liu[34,j,k], Y. Liu[34,j,k], Y. B. Liu[39], Z. A. Liu[1,53,58], Z. Q. Liu[45], X. C. Lou[1,53,58], F. X. Lu[54], H. J. Lu[21], J. G. Lu[1,53], X. L. Lu[1], Y. Lu[7], Y. P. Lu[1,53], Z. H. Lu[1], C. L. Luo[37], M. X. Luo[74], T. Luo[10,f], X. L. Luo[1,53], X. R. Lyu[58], Y. F. Lyu[39], F. C. Ma[36], H. L. Ma[1], L. L. Ma[45], M. M. Ma[1,58], Q. M. Ma[1], R. Q. Ma[1,58], R. T. Ma[58], X. Y. Ma[1,53], Y. Ma[42,g], F. E. Maas[17], M. Maggiora[69A,69C], S. Maldaner[4], S. Malde[64], Q. A. Malik[68], A. Mangoni[26B], Y. J. Mao[42,g], Z. P. Mao[1], S. Marcello[69A,69C], Z. X. Meng[61], J. Messchendorp[12,59], G. Mezzadri[27A], H. Miao[1], T. J. Min[38], R. E. Mitchell[25], X. H. Mo[1,53,58], N. Yu. Muchnoi[11,b], Y. Nefedov[32], F. Nerling[17,d], I. B. Nikolaev[11,b], Z. Ning[1,53], S. Nisar[9,l], Y. Niu [45], S. L. Olsen[58], Q. Ouyang[1,53,58], S. Pacetti[26B,26C], X. Pan[10,f], Y. Pan[52], A. Pathak[30], M. Pelizaeus[4], H. P. Peng[66,53], K. Peters[12,d], J. L. Ping[37], R. G. Ping[1,58], S. Plura[31], S. Pogodin[32], V. Prasad[66,53], F. Z. Qi[1], H. Qi[66,53], H. R. Qi[56], M. Qi[38], T. Y. Qi[10,f], S. Qian[1,53], W. B. Qian[58], Z. Qian[54], C. F. Qiao[58], J. J. Qin[67], L. Q. Qin[13], X. P. Qin[10,f], X. S. Qin[45], Z. H. Qin[1,53], J. F. Qiu[1], S. Q. Qu[56], K. H. Rashid[68], C. F. Redmer[31], K. J. Ren[35], A. Rivetti[69C], V. Rodin[59], M. Rolo[69C], G. Rong[1,58], Ch. Rosner[17], S. N. Ruan[39], H. S. Sang[66], A. Sarantsev[32,c], Y. Schelhaas[31], C. Schnier[4], K. Schoenning[70], M. Scodeggio[27A,27B], K. Y. Shan[10,f], W. Shan[22], X. Y. Shan[66,53], J. F. Shangguan[50], L. G. Shao[1,58], M. Shao[66,53], C. P. Shen[10,f], H. F. Shen[1,58], X. Y. Shen[1,58], B. A. Shi[58], H. C. Shi[66,53], J. Y. Shi[1], Q. Q. Shi[50], R. S. Shi[1,58], X. Shi[1,53], X. D Shi[66,53], J. J. Song[18], W. M. Song[30,1], Y. X. Song[42,g], S. Sosio[69A,69C], S. Spataro[69A,69C], F. Stieler[31], K. X. Su[71], P. P. Su[50], Y. J. Su[58], G. X. Sun[1], H. Sun[58], H. K. Sun[1], J. F. Sun[18], L. Sun[71], S. S. Sun[1,58], T. Sun[1,58], W. Y. Sun[30], X Sun[23,h], Y. J. Sun[66,53], Y. Z. Sun[1], Z. T. Sun[45], Y. H. Tan[71], Y. X. Tan[66,53], C. J. Tang[49], G. Y. Tang[1], J. Tang[54], L. Y Tao[67], Q. T. Tao[23,h], M. Tat[64], J. X. Teng[66,53], V. Thoren[70], W. H. Tian[47], Y. Tian[28,58], I. Uman[57B], B. Wang[1], B. L. Wang[58], C. W. Wang[38], D. Y. Wang[42,g], F. Wang[67], H. J. Wang[34,j,k], H. P. Wang[1,58], K. Wang[1,53], L. L. Wang[1], M. Wang[45], M. Z. Wang[42,g], Meng Wang[1,58], S. Wang[13], S. Wang[10,f], T. Wang[10,f], T. J. Wang[39], W. Wang[54], W. H. Wang[71], W. P. Wang[66,53], X. Wang[42,g], X. F. Wang[34,j,k], X. L. Wang[10,f], Y. Wang[56], Y. D. Wang[41], Y. F. Wang[1,53,58], Y. H. Wang[43], Y. Q. Wang[1], Yaqian Wang[16,1], Z. Wang[1,53], Z. Y. Wang[1,58], Ziyi Wang[58], D. H. Wei[13], F. Weidner[63], S. P. Wen[1], D. J. White[62], U. Wiedner[4], G. Wilkinson[64], M. Wolke[70], L. Wollenberg[4], J. F. Wu[1,58], L. H. Wu[1], L. J. Wu[1,58], X. Wu[10,f], X. H. Wu[30], Y. Wu[66], Y. J Wu[28], Z. Wu[1,53], L. Xia[66,53], T. Xiang[42,g], D. Xiao[34,j,k], G. Y. Xiao[38], H. Xiao[10,f], S. Y. Xiao[1], Y. L. Xiao[10,f], Z. J. Xiao[37], C. Xie[38], X. H. Xie[42,g], Y. Xie[45], Y. G. Xie[1,53], Y. H. Xie[6], Z. P. Xie[66,53], T. Y. Xing[1,58], C. F. Xu[1], C. J. Xu[54], G. F. Xu[1], H. Y. Xu[61], Q. J. Xu[15], X. P. Xu[50], Y. C. Xu[58], Z. P. Xu[38], F. Yan[10,f], L. Yan[10,f], W. B. Yan[66,53], W. C. Yan[75], H. J. Yang[46,e], H. L. Yang[30], H. X. Yang[1], L. Yang[47], S. L. Yang[58], Tao Yang[1], Y. F. Yang[39], Y. X. Yang[1,58], Yifan Yang[1,58], M. Ye[1,53], M. H. Ye[8], J. H. Yin[1], Z. Y. You[54], B. X. Yu[1,53,58], C. X. Yu[39], G. Yu[1,58], T. Yu[67], X. D. Yu[42,g], C. Z. Yuan[1,58], L. Yuan[2], S. C. Yuan[1], X. Q. Yuan[1], Y. Yuan[1,58], Z. Y. Yuan[54], C. X. Yue[35], A. A. Zafar[68], F. R. Zeng[45], X. Zeng[6], Y. Zeng[23,h], Y. H. Zhan[54], A. Q. Zhang[1], B. L. Zhang[1], B. X. Zhang[1], D. H. Zhang[39], G. Y. Zhang[18], H. Zhang[66], H. H. Zhang[54], H. H. Zhang[30], H. Y. Zhang[1,53], J. L. Zhang[72], J. Q. Zhang[37], J. W. Zhang[1,53,58], J. X. Zhang[34,j,k], J. Y. Zhang[1], J. Z. Zhang[1,58], Jianyu Zhang[1,58], Jiawei Zhang[1,58], L. M. Zhang[56], L. Q. Zhang[54], Lei Zhang[38], P. Zhang[1], Q. Y. Zhang[35,75], Shuihan Zhang[1,58], Shulei Zhang[23,h], X. D. Zhang[41],

X. M. Zhang[1], X. Y. Zhang[50], X. Y. Zhang[45], Y. Zhang[64], Y. T. Zhang[75], Y. H. Zhang[1,53], Yan Zhang[66,53], Yao Zhang[1], Z. H. Zhang[1], Z. Y. Zhang[71], Z. Y. Zhang[39], G. Zhao[1], J. Zhao[35], J. Y. Zhao[1,58], J. Z. Zhao[1,53], Lei Zhao[66,53], Ling Zhao[1], M. G. Zhao[39], Q. Zhao[1], S. J. Zhao[75], Y. B. Zhao[1,53], Y. X. Zhao[28,58], Z. G. Zhao[66,53], A. Zhemchugov[32,a], B. Zheng[67], J. P. Zheng[1,53], Y. H. Zheng[58], B. Zhong[37], C. Zhong[67], X. Zhong[54], H. Zhou[45], L. P. Zhou[1,58], X. Zhou[71], X. K. Zhou[58], X. R. Zhou[66,53], X. Y. Zhou[35], Y. Z. Zhou[10,f], J. Zhu[39], K. Zhu[1], K. J. Zhu[1,53,58], L. X. Zhu[58], S. H. Zhu[65], S. Q. Zhu[38], T. J. Zhu[72], W. J. Zhu[10,f], Y. C. Zhu[66,53], Z. A. Zhu[1,58], B. S. Zou[1], J. H. Zou[1]

(BESIII Collaboration)

[1] *Institute of High Energy Physics, Beijing 100049, People's Republic of China*
[2] *Beihang University, Beijing 100191, People's Republic of China*
[3] *Beijing Institute of Petrochemical Technology, Beijing 102617, People's Republic of China*
[4] *Bochum Ruhr-University, D-44780 Bochum, Germany*
[5] *Carnegie Mellon University, Pittsburgh, Pennsylvania 15213, USA*
[6] *Central China Normal University, Wuhan 430079, People's Republic of China*
[7] *Central South University, Changsha 410083, People's Republic of China*
[8] *China Center of Advanced Science and Technology, Beijing 100190, People's Republic of China*
[9] *COMSATS University Islamabad, Lahore Campus, Defence Road, Off Raiwind Road, 54000 Lahore, Pakistan*
[10] *Fudan University, Shanghai 200433, People's Republic of China*
[11] *G.I. Budker Institute of Nuclear Physics SB RAS (BINP), Novosibirsk 630090, Russia*
[12] *GSI Helmholtzcentre for Heavy Ion Research GmbH, D-64291 Darmstadt, Germany*
[13] *Guangxi Normal University, Guilin 541004, People's Republic of China*
[14] *Guangxi University, Nanning 530004, People's Republic of China*
[15] *Hangzhou Normal University, Hangzhou 310036, People's Republic of China*
[16] *Hebei University, Baoding 071002, People's Republic of China*
[17] *Helmholtz Institute Mainz, Staudinger Weg 18, D-55099 Mainz, Germany*
[18] *Henan Normal University, Xinxiang 453007, People's Republic of China*
[19] *Henan University of Science and Technology, Luoyang 471003, People's Republic of China*
[20] *Henan University of Technology, Zhengzhou 450001, People's Republic of China*
[21] *Huangshan College, Huangshan 245000, People's Republic of China*
[22] *Hunan Normal University, Changsha 410081, People's Republic of China*
[23] *Hunan University, Changsha 410082, People's Republic of China*
[24] *Indian Institute of Technology Madras, Chennai 600036, India*
[25] *Indiana University, Bloomington, Indiana 47405, USA*
[26] *INFN Laboratori Nazionali di Frascati, (A)INFN Laboratori Nazionali di Frascati, I-00044, Frascati, Italy; (B)INFN Sezione di Perugia, I-06100, Perugia, Italy; (C)University of Perugia, I-06100, Perugia, Italy*
[27] *INFN Sezione di Ferrara, (A)INFN Sezione di Ferrara, I-44122, Ferrara, Italy; (B)University of Ferrara, I-44122, Ferrara, Italy*
[28] *Institute of Modern Physics, Lanzhou 730000, People's Republic of China*
[29] *Institute of Physics and Technology, Peace Avenue 54B, Ulaanbaatar 13330, Mongolia*
[30] *Jilin University, Changchun 130012, People's Republic of China*
[31] *Johannes Gutenberg University of Mainz, Johann-Joachim-Becher-Weg 45, D-55099 Mainz, Germany*
[32] *Joint Institute for Nuclear Research, 141980 Dubna, Moscow region, Russia*
[33] *Justus-Liebig-Universitaet Giessen, II. Physikalisches Institut, Heinrich-Buff-Ring 16, D-35392 Giessen, Germany*
[34] *Lanzhou University, Lanzhou 730000, People's Republic of China*
[35] *Liaoning Normal University, Dalian 116029, People's Republic of China*
[36] *Liaoning University, Shenyang 110036, People's Republic of China*
[37] *Nanjing Normal University, Nanjing 210023, People's Republic of China*
[38] *Nanjing University, Nanjing 210093, People's Republic of China*
[39] *Nankai University, Tianjin 300071, People's Republic of China*
[40] *National Centre for Nuclear Research, Warsaw 02-093, Poland*
[41] *North China Electric Power University, Beijing 102206, People's Republic of China*
[42] *Peking University, Beijing 100871, People's Republic of China*
[43] *Qufu Normal University, Qufu 273165, People's Republic of China*
[44] *Shandong Normal University, Jinan 250014, People's Republic of China*
[45] *Shandong University, Jinan 250100, People's Republic of China*
[46] *Shanghai Jiao Tong University, Shanghai 200240, People's Republic of China*
[47] *Shanxi Normal University, Linfen 041004, People's Republic of China*
[48] *Shanxi University, Taiyuan 030006, People's Republic of China*
[49] *Sichuan University, Chengdu 610064, People's Republic of China*
[50] *Soochow University, Suzhou 215006, People's Republic of China*
[51] *South China Normal University, Guangzhou 510006, People's Republic of China*
[52] *Southeast University, Nanjing 211100, People's Republic of China*
[53] *State Key Laboratory of Particle Detection and Electronics, Beijing 100049, Hefei 230026, People's Republic of China*
[54] *Sun Yat-Sen University, Guangzhou 510275, People's Republic of China*

[55] Suranaree University of Technology, University Avenue 111, Nakhon Ratchasima 30000, Thailand
[56] Tsinghua University, Beijing 100084, People's Republic of China
[57] Turkish Accelerator Center Particle Factory Group, (A)Istinye University, 34010, Istanbul, Turkey; (B)Near East University, Nicosia, North Cyprus, Mersin 10, Turkey
[58] University of Chinese Academy of Sciences, Beijing 100049, People's Republic of China
[59] University of Groningen, NL-9747 AA Groningen, The Netherlands
[60] University of Hawaii, Honolulu, Hawaii 96822, USA
[61] University of Jinan, Jinan 250022, People's Republic of China
[62] University of Manchester, Oxford Road, Manchester, M13 9PL, United Kingdom
[63] University of Muenster, Wilhelm-Klemm-Strasse 9, 48149 Muenster, Germany
[64] University of Oxford, Keble Road, Oxford OX13RH, United Kingdom
[65] University of Science and Technology Liaoning, Anshan 114051, People's Republic of China
[66] University of Science and Technology of China, Hefei 230026, People's Republic of China
[67] University of South China, Hengyang 421001, People's Republic of China
[68] University of the Punjab, Lahore-54590, Pakistan
[69] University of Turin and INFN, (A)University of Turin, I-10125, Turin, Italy; (B)University of Eastern Piedmont, I-15121, Alessandria, Italy; (C)INFN, I-10125, Turin, Italy
[70] Uppsala University, Box 516, SE-75120 Uppsala, Sweden
[71] Wuhan University, Wuhan 430072, People's Republic of China
[72] Xinyang Normal University, Xinyang 464000, People's Republic of China
[73] Yunnan University, Kunming 650500, People's Republic of China
[74] Zhejiang University, Hangzhou 310027, People's Republic of China
[75] Zhengzhou University, Zhengzhou 450001, People's Republic of China

[a] Also at the Moscow Institute of Physics and Technology, Moscow 141700, Russia
[b] Also at the Novosibirsk State University, Novosibirsk, 630090, Russia
[c] Also at the NRC "Kurchatov Institute", PNPI, 188300, Gatchina, Russia
[d] Also at Goethe University Frankfurt, 60323 Frankfurt am Main, Germany
[e] Also at Key Laboratory for Particle Physics, Astrophysics and Cosmology, Ministry of Education; Shanghai Key Laboratory for Particle Physics and Cosmology; Institute of Nuclear and Particle Physics, Shanghai 200240, People's Republic of China
[f] Also at Key Laboratory of Nuclear Physics and Ion-beam Application (MOE) and Institute of Modern Physics, Fudan University, Shanghai 200443, People's Republic of China
[g] Also at State Key Laboratory of Nuclear Physics and Technology, Peking University, Beijing 100871, People's Republic of China
[h] Also at School of Physics and Electronics, Hunan University, Changsha 410082, China
[i] Also at Guangdong Provincial Key Laboratory of Nuclear Science, Institute of Quantum Matter, South China Normal University, Guangzhou 510006, China
[j] Also at Frontiers Science Center for Rare Isotopes, Lanzhou University, Lanzhou 730000, People's Republic of China
[k] Also at Lanzhou Center for Theoretical Physics, Lanzhou University, Lanzhou 730000, People's Republic of China
[l] Also at the Department of Mathematical Sciences, IBA, Karachi, Pakistan

Based on 7.33 fb^{-1} of e^+e^- collision data taken at center-of-mass energies between 4.128 and 4.226 GeV with the BESIII detector, we measure the branching fraction of $D_s^{*+} \to D_s^+\pi^0$ relative to that of $D_s^{*+} \to D_s^+\gamma$ to be $(6.16 \pm 0.43 \pm 0.19)\%$. The first uncertainty is statistical and the second one is systematic. By using the world average value of the branching fraction of $D_s^{*+} \to D_s^+ e^+e^-$, we determine the branching fractions of $D_s^{*+} \to D_s^+\gamma$ and $D_s^{*+} \to D_s^+\pi^0$ to be $(93.57 \pm 0.44 \pm 0.19)\%$ and $(5.76 \pm 0.44 \pm 0.19)\%$, respectively.

I. INTRODUCTION

The excited strange charmed meson, D_s^{*+}, is formed from $c\bar{s}$ quark-antiquark pair. Throughout this paper, charge-conjugate states are always included. The D_s^{*+} decays are dominated by the radiative process $D_s^{*+} \to D_s^+\gamma$ and the isospin-violating hadronic process $D_s^{*+} \to D_s^+\pi^0$ due to the quark SU(2) flavor breaking and isospin violating effects. Measurements of the branching fractions (BFs) of the D_s^{*+} decays are important to explore quantum chromodynamics (QCD) [1] describing the strong interaction. The decay widths of $D_s^{*+} \to D_s^+\gamma$ and/or $D_s^{*+} \to D_s^+\pi^0$ have been theoretically predicted based on effective models, e.g. chiral perturbation theory (χPT) [2–5], the light-front quark model (LFQM) [6], the relativistic quark model (RQM)[7], QCD sum rules (QCDSR) [8, 9], the Nambu-Jona-Lasinio model (NJLM) [10], lattice QCD (LQCD) [11], the non-relativistic quark model (NRQM) [12, 13], and the covariant model (CM) [14]. The BF of $D_s^{*+} \to D_s^+\pi^0$ relative to that of $D_s^{*+} \to D_s^+\gamma$ has been measured by using e^+e^- collision data accumulated at the $\Upsilon(3S)$ and $\Upsilon(4S)$ by the CLEO [15] and BaBar [16] experiments. The precision of the world average of the BF of $D_s^{*+} \to D_s^+\gamma$ is about 0.7% [17]. Precision measurements of these BFs help to constrain the model parameters, thereby improving the effective models. In addition, the BFs are important inputs in the precise determination of the D_s^+ decay constant $f_{D_s^+}$ and the $c \to s$ CKM matrix element $|V_{cs}|$ via the $e^+e^- \to D_s^{*\pm} D_s^{\mp}$ processes.

In this paper, we report an improved measurement of the BF of $D_s^{*+} \to D_s^+ \pi^0$ relative to $D_s^{*+} \to D_s^+ \gamma$ and then determine the BFs of $D_s^{*+} \to D_s^+ \gamma$ and $D_s^{*+} \to D_s^+ \pi^0$. This analysis is carried out by using 7.33 fb^{-1} of e^+e^- collision data taken at center-of-mass energies $E_{\rm cm}$ between 4.128 and 4.226 GeV with the BESIII detector.

II. BESIII DETECTOR AND MONTE CARLO

The BESIII detector [18] records symmetric e^+e^- collisions provided by the BEPCII storage ring [19] in the center-of-mass energy range from 2.0 to 4.95 GeV, with a peak luminosity of 1×10^{33} $\mathrm{cm}^{-2}\mathrm{s}^{-1}$ achieved at $\sqrt{s}$ = 3.773 GeV. BESIII has collected large data samples in this energy region [20]. BESIII is a cylindrical spectrometer with a geometrical acceptance of 93% over the 4π solid angle. It consists of a helium-based multilayer drift chamber (MDC), a plastic scintillator time-of-flight system (TOF), and a CsI(Tl) electromagnetic calorimeter (EMC), which are all enclosed in a superconducting solenoidal magnet providing a 1.0 T magnetic field. The solenoid is supported by an octagonal flux-return yoke with resistive plate counter muon identifier modules interleaved with steel [21]. The charged particle momentum resolution is 0.5% at 1 GeV/c, and the specific energy loss ($\mathrm{d}E/\mathrm{d}x$) resolution is 6% for the electrons from Bhabha scattering. The EMC measures photon energies with a resolution of 2.5% (5%) at 1 GeV in the barrel (end-cap) region. The time resolution in the TOF barrel region is 68 ps. The end-cap TOF system was upgraded in 2015 using multi-gap resistive plate chamber technology, providing a time resolution of 60 ps [22]. Approximately 83% of the data used here was collected after this upgrade; luminosities [23] at each energy are given in Table 1.

Simulated data samples are produced with a GEANT4-based [24] Monte Carlo (MC) toolkit including the geometric description of the BESIII detector and the detector response. The simulation includes the beam energy spread and initial state radiation (ISR) in the e^+e^- annihilations with the generator KKMC [25]. In the MC simulation, the production of open-charm processes directly produced via e^+e^- annihilations are modelled with the generator CONEXC [26]. The ISR production of vector charmonium(-like) states and the continuum processes are incorporated in KKMC [25]. All particle decays are modelled with EVTGEN [27] using BFs either taken from the Particle Data Group [17], when available, or otherwise estimated with LUNDCHARM [28]. Final state radiation (FSR) from charged final state particles is incorporated using PHOTOS [29].

The input cross section line shape of $e^+e^- \to D_s^{*\pm} D_s^{\mp}$ is based on the results in Ref. [30]. In this analysis, the inclusive MC sample, which is generated at various energy points and has an integrated luminosity of 40 times individual data sets, is used to determine detection efficiencies and to estimate background contributions.

III. EVENT SELECTION

At the center-of-mass energies between 4.128 and 4.226 GeV, $D_s^{*+} D_s^-$ pairs are produced copiously by e^+e^- collisions. The D_s^{*+} mesons decay predominantly via $D_s^{*+} \to D_s^+ \gamma$ and $D_s^{*+} \to D_s^+ \pi^0$. Candidate events are selected by reconstructing D_s^+ and D_s^- mesons via hadronic decay modes. To obtain better momentum resolution and lower background contamination, we use three modes of $D_s^+ \to K^+K^-\pi^+$ versus $D_s^- \to K^+K^-\pi^-$, $D_s^+ \to K^+K^-\pi^+$ versus $D_s^- \to K_S^0 K^-$, and $D_s^+ \to K_S^0 K^+$ versus $D_s^- \to K_S^0 K^-$, which are labelled as modes I, II, and III, respectively. In order to improve detection efficiencies, no transition photon or π^0 from the D_s^{*+} decay is required.

Charged tracks detected in the MDC are required to be within a polar angle (θ) range of $|\cos\theta| < 0.93$, where θ is defined with respect to the z-axis, which is the symmetry axis of the MDC. For charged tracks not originating from K_S^0 decays, the distance of closest approach to the interaction point (IP) must be less than 10 cm along the z-axis, $|V_z|$, and less than 1 cm in the transverse plane, $|V_{xy}|$. No additional charged track passing the $\cos\theta$ and IP cuts is allowed for selected candidates. Particle identification (PID) for charged tracks combines measurements of the $\mathrm{d}E/\mathrm{d}x$ in the MDC and the flight time in the TOF to form likelihoods for charged pion and kaon hypotheses, $\mathcal{L}(\pi)$ and $\mathcal{L}(K)$. Pion candidates are required to satisfy $\mathcal{L}(\pi) > \mathcal{L}(K)$ and $\mathcal{L}(\pi) > 0$, and kaon candidates are required to satisfy $\mathcal{L}(K) > \mathcal{L}(\pi)$ and $\mathcal{L}(K) > 0$.

The K_S^0 candidates are reconstructed via the decay $K_S^0 \to \pi^+\pi^-$. The two charged pions are required to satisfy $|V_z| < 20$ cm and $|\cos\theta| < 0.93$ but no particle identification is applied. The $\pi^+\pi^-$ invariant mass is required to be within the interval $(0.487, 0.511)$ GeV/c^2. A vertex fit is performed, constraining the two tracks to originate from a common vertex, and the decay length of K_S^0 candidates is required to be greater than twice the resolution.

To suppress non-$D_s^{\pm} D_s^{*\mp}$ events, the beam-constrained mass of the D_s^- candidate

$$M_{\rm BC} \equiv \sqrt{E_{\rm beam}^2 - |\vec{p}_{\rm tag}|^2}, \tag{1}$$

is required to be within the intervals as shown in Table 1. Here, $E_{\rm beam}$ is the beam energy and $\vec{p}_{\rm tag}$ is the three-momentum of the reconstructed D_s^- candidate in the e^+e^- center-of-mass frame. In each event, we only keep one candidate per tag mode per charge, selecting the one

Table 1. The integrated luminosity and $M_{\rm BC}$ requirement for each energy ($E_{\rm cm}$) point.

$E_{\rm cm}$ (GeV)	Luminosity (pb^{-1})	$M_{\rm BC}$ (GeV/c^2)
4.128	401.5	[2.010, 2.061]
4.157	408.7	[2.010, 2.070]
4.178	3189.0	[2.010, 2.073]
4.189	569.8	[2.010, 2.076]
4.199	526.0	[2.010, 2.079]
4.209	571.7	[2.010, 2.082]
4.219	568.7	[2.010, 2.085]
4.226	1091.7	[2.010, 2.088]

with the D_s^- recoil mass

$$M_{\rm rec} \equiv \sqrt{(E_{\rm cm} - \sqrt{|\vec{p}_{\rm tag}|^2 + m^2_{D_s}})^2 - |\vec{p}_{\rm tag}|^2}, \quad (2)$$

closest to the nominal D_s^{*+} mass [17]. The D_s^+ candidate is selected in the presence of the tag D_s^-. If there are multiple D_s^+ combinations in an event, the one giving the minimum $|M_{D_s^+} + M_{D_s^-} - 2m_{D_s}|$ is retained for further analysis. Here $M_{D_s^\pm}$ is the invariant mass of the $D_s^\pm$ candidate and m_{D_s} is the nominal D_s mass [17]. Figure 1 shows the distribution of $M_{D_s^-}$ vs. $M_{D_s^+}$ of the accepted candidates in data. To suppress background, the invariant masses of $K^+K^-\pi^\pm$ and $K^0_S K^\pm$ combinations are required to be within the interval $M_{D_s^\pm} \in (1.958, 1.978)$ GeV/c^2.

To improve momentum resolution, a two-constraint (2C) kinematic fit, in which the invariant mass of the $K^+K^-\pi^\pm$ or $K^0_S K^\pm$ combination is constrained to the known D_s mass [17] is performed. The momenta updated by the kinematic fit are kept for further analysis.

To separate the $D_s^{*+} \to D_s^+\gamma$ and $D_s^{*+} \to D_s^+\pi^0$ candidates, we define the missing mass squared of the reconstructed $D_s^+D_s^-$ combination as

$$M^2_{\rm miss} \equiv \left(E_{\rm cm} - E_{D_s^+} - E_{D_s^-}\right)^2 - |-\vec{p}_{D_s^+} - \vec{p}_{D_s^-}|^2, \quad (3)$$

where $E_{D_s^\pm}$ and $\vec{p}_{D_s^\pm}$ are the energy and momentum of $D_s^\pm$ in the e^+e^- center-of-mass system, respectively. The resultant $M^2_{\rm miss}$ distribution of the accepted $D_s^+D_s^-$ candidate combinations is shown in Fig. 2, where the peak near to zero and its right-side peak correspond to $D_s^{*+} \to D_s^+\gamma$ and $D_s^{*+} \to D_s^+\pi^0$ candidates, respectively.

IV. BRANCHING FRACTIONS

Following Ref. [31], the BF of $D_s^{*+} \to D_s^+\gamma$ relative to the sum of $D_s^{*+} \to D_s^+\gamma$ and $D_s^{*+} \to D_s^+\pi^0$ is determined

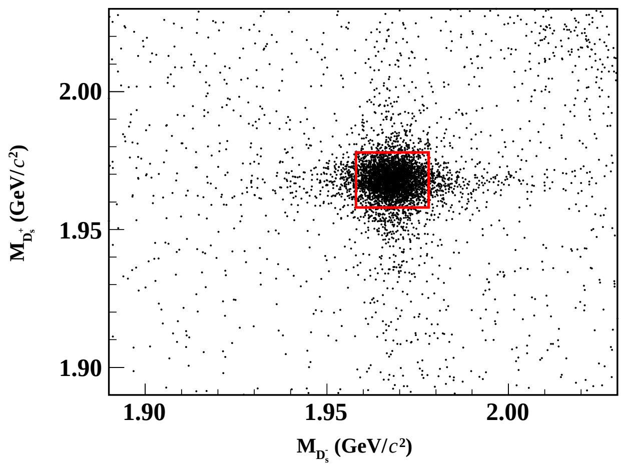

Fig. 1. The distribution of $M_{D_s^-}$ vs. $M_{D_s^+}$ summing over modes I, II, and III in data. The red rectangle denotes the signal region.

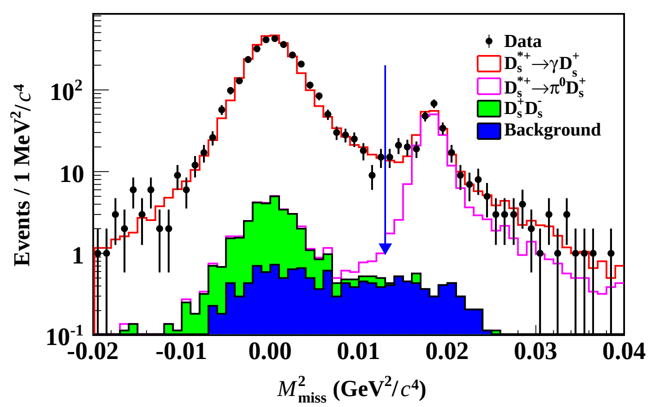

Fig. 2. The $M^2_{\rm miss}$ distributions of the accepted candidates, summing over modes I, II, and III. The points with error bars are data, the open red histograms are the scaled signal MC events, and the filled green histograms are normalized background events from the inclusive MC sample. The blue vertical arrow shows the dividing line for $D_s^{*+} \to D_s^+\gamma$ and $D_s^{*+} \to D_s^+\pi^0$ candidates; for the filled green histogram, the small peaking background around zero is from the $e^+e^- \to D_s^+D_s^-$ process, and the open red and magenta histograms are the signals of $D_s^{*+} \to D_s^+\gamma$ and $D_s^{*+} \to D_s^+\pi^0$, respectively.

by

$$f_\gamma = \frac{\mathcal{B}_{D_s^{*+}\to D_s^+\gamma}}{\mathcal{B}_{D_s^{*+}\to D_s^+\gamma} + \mathcal{B}_{D_s^{*+}\to D_s^+\pi^0}} = \frac{N_\gamma^{\rm prod}}{N_\gamma^{\rm prod} + N_{\pi^0}^{\rm prod}}, \quad (4)$$

where $N_\gamma^{\rm prod}$ and $N_{\pi^0}^{\rm prod}$ are the numbers of produced $D_s^{*+} \to D_s^+\gamma$ and $D_s^{*+} \to D_s^+\pi^0$ events, respectively. This ratio captures the binomial nature of the separation of the low-background signal into the two decays under study.

As shown in Fig. 2, the individual signal regions of

$M^2_{\rm miss}$ are defined as $[-0.020, 0.013]$ and $[0.013, 0.040]$ GeV^2/c^4 for $D_s^{*+} \to D_s^+\gamma$ and $D_s^{*+} \to D_s^+\pi^0$, respectively. The dividing line accepts about 99.0% of the $D^{*+} \to D_s^+\gamma$ signal and about 98.5% of the $D_s^{*+} \to D_s^+\pi^0$ signal. Due to the overlapping $M^2_{\rm miss}$ distributions, some $D_s^{*+} \to D_s^+\gamma$ events can be misidentified as $D_s^{*+} \to D_s^+\pi^0$, and vice versa. To account for this effect, the yields of $N_\gamma^{\rm prod}$ and $N_{\pi^0}^{\rm prod}$ are obtained by solving the following equation

$$\begin{pmatrix} N_\gamma^{\rm obs} - N_\gamma^{\rm bkg} \\ N_{\pi^0}^{\rm obs} - N_{\pi^0}^{\rm bkg} \end{pmatrix} = \begin{pmatrix} \epsilon_{\gamma\gamma} & \epsilon_{\pi^0\gamma} \\ \epsilon_{\gamma\pi^0} & \epsilon_{\pi^0\pi^0} \end{pmatrix} \begin{pmatrix} N_\gamma^{\rm prod} \\ N_{\pi^0}^{\rm prod} \end{pmatrix}, \quad (5)$$

where $N_i^{\rm obs}$ is the number of selected events in data by counting, $N_i^{\rm bkg}$ is the number of background events estimated from the inclusive MC sample; ϵ_{ij} is the efficiency of the generated $D_s^{*+} \to D_s^+ + i$ events selected as $D_s^{*+} \to D_s^+ + j$, where i and j denote γ or π^0. Both $D_s^{*+} \to D_s^+\pi^0, D_s^+\gamma$ are simulated. The background rates estimated from the inclusive MC sample for modes I, II, and III are all less than 1.5%.

To consider different detection efficiencies for ISR and FSR effects, the detection efficiencies at various energy points have been weighted by individual single tag D_s^+ yields in data.

Table 2 lists the quantities used for the f_γ measurements and the results obtained. Weighting the f_γ results for modes I, II, and III by their inverse statistical uncertainties squared, we obtain their average $f_\gamma = (94.20 \pm 0.38)\%$.

V. SYSTEMATIC UNCERTAINTIES

The systematic uncertainties in the BF measurements are discussed below. The systematic uncertainty due to $M^2_{\rm miss}$ resolution is examined in the following procedure. We perform a fit to $M^2_{\rm miss}$ distribution of data. To take into account the resolution difference between data and MC, a signal MC shape smeared with a Gaussian function is used. From the fit, we obtain the parameters (means, widths) of the Gaussian resolution functions, which are $(1.0 \pm 0.1, 1.0 \pm 0.2)$, $(1.1 \pm 0.1, 1.0 \pm 0.2)$, and $(0.4 \pm 0.3, 1.7 \pm 0.4)$ MeV^2/c^4 for modes I, II, and III, respectively. The change of BF before and after smearing the Gaussian resolution function to the $M^2_{\rm miss}$ distribution of the signal MC events, 0.07%, is taken as the associated systematic uncertainty.

The systematic uncertainty caused by the statistical uncertainty of the MC efficiencies is estimated by varying each of the efficiency matrix elements by $\pm 1\sigma$. The largest change of the BF is taken as the systematic uncertainty.

The systematic uncertainty from background estimation is considered in two parts. The number of background events is calculated from the inclusive MC sample. The corresponding systematic uncertainty is estimated from the uncertainties of the cross sections used in generating this sample. The dominant background events are from open charm processes of $e^+e^- \to D_s^+D_s^-$ and $e^+e^- \to D_s^{*+}D_s^-$. The systematic uncertainty is estimated by varying the cross sections and BFs of the hadronic D_s^+ decays by $\pm 1\sigma$. This effect on the BF measurement is negligible. In addition, we have also varied the simulated background events by the ratio of the background events observed in the $D_s^+D_s^-$ sideband regions between data and the inclusive MC sample. The change of the BF, 0.10%, is taken as the corresponding systematic uncertainty.

Other possible systematic uncertainty sources, such as the ISR simulation, the kinematic fit, the tracking and the particle identification efficiencies between the two decay modes of D_s^{*+}, the $M_{\rm BC}$ requirement and the $M^2_{\rm miss}$ range, have also been investigated. All of them are negligible.

All systematic uncertainties are summarized in Table 3. Assuming the systematic uncertainties from different sources are independent, the total systematic uncertainty is obtained to be 0.17% by adding all the sources quadratically.

VI. SUMMARY

By analyzing 7.33 fb^{-1} of e^+e^- collision data taken at center-of-mass energies between 4.128 and 4.226 GeV, we measure the BF of $D_s^{*+} \to D_s^+\gamma$ relative to the sum of $D_s^{*+} \to D_s^+\gamma$ and $D_s^{*+} \to D_s^+\pi^0$ to be $f_\gamma = (94.20 \pm 0.38 \pm 0.17)\%$. This gives the BF of $D_s^{*+} \to D_s^+\pi^0$ relative to that of $D_s^{*+} \to D_s^+\gamma$ to be $\mathcal{B}_{D_s^{*+}\to D_s^+\pi^0}/\mathcal{B}_{D_s^{*+}\to D_s^+\gamma} = \frac{1}{f_\gamma} - 1 = (6.16 \pm 0.43 \pm 0.19)\%$. The D_s^{*+} is known to decay dominantly into three final states of $D_s^+\gamma$, $D_s^+\pi^0$ and $D_s^+e^+e^-$ [14]. Combining the world average of $\mathcal{B}_{D_s^{*+}\to D_s^+e^+e^-} = (0.67 \pm 0.16)\%$ [17], we obtain $\mathcal{B}_{D_s^{*+}\to D_s^+\gamma} = (93.57 \pm 0.44 \pm 0.19)\%$ and $\mathcal{B}_{D_s^{*+}\to D_s^+\pi^0} = (5.76 \pm 0.44 \pm 0.19)\%$.

Figure 3 shows the comparison of the measured BF of $\mathcal{B}_{D_s^{*+}\to D_s^+\pi^0}/\mathcal{B}_{D_s^{*+}\to D_s^+\gamma}$ with other experiments and the world average value [17]. Our measurement is well consistent with the previous ones but with better precision. Table 4 shows comparisons of the BFs measured in this work with the world average values and the decay widths or BFs predicted by various theories. Our results of $\mathcal{B}_{D_s^*\to D_s^+\gamma}$ and $\mathcal{B}_{D_s^*\to D_s^+\pi^0}$ are consistent with those predicted in Ref. [14]. At present, only limits on the D_s^{*+} width have been reported. More experimental measurements and theoretical calculations of the D_s^{*+} decays will be beneficial to give quantitative tests on the predicted partial decay widths, thereby better understand the radiative and strong decays of D_s^{*+}. As necessary inputs, the reported BFs with much improved precision are also important for the precise measurements of $f_{D_s^+}$ and $|V_{cs}|$ by using the reactions of $e^+e^- \to D_s^{*\pm}D_s^{\mp}$.

Table 2. The quantities used for f_γ measurements and the obtained results. The average result is weighted over modes I, II, and III by their inverse statistical uncertainties squared. The uncertainties are statistical only.

Mode	$N_\gamma^{\rm obs}$	$N_{\pi^0}^{\rm obs}$	$N_\gamma^{\rm bkg}$	$N_{\pi^0}^{\rm bkg}$	$\epsilon_{\gamma\gamma}$ (%)	$\epsilon_{\gamma\pi^0}$ (%)	$\epsilon_{\pi^0\gamma}$ (%)	$\epsilon_{\pi^0\pi^0}$ (%)	f_γ (%)
I	2293.0 ± 47.9	239.0 ± 15.5	31.0 ± 0.9	5.0 ± 0.4	14.16 ± 0.04	0.42 ± 0.01	0.22 ± 0.02	15.08 ± 0.17	93.52 ± 0.49
II	1044.0 ± 32.3	83.0 ± 9.1	12.0 ± 0.5	1.0 ± 0.2	15.97 ± 0.07	0.46 ± 0.01	0.16 ± 0.03	16.38 ± 0.29	95.32 ± 0.63
III	119.0 ± 10.9	11.0 ± 3.3	1.0 ± 0.2	0.0 ± 0.0	17.27 ± 0.23	0.52 ± 0.05	0.00 ± 0.00	18.08 ± 0.96	94.31 ± 2.04
Average									94.20 ± 0.38

Table 3. Relative systematic uncertainties in the determination of f_γ.

Source	Uncertainty (%)
$M^2_{\rm miss}$ resolution	0.07
MC statistics	0.12
Background	0.10
Sum	0.17

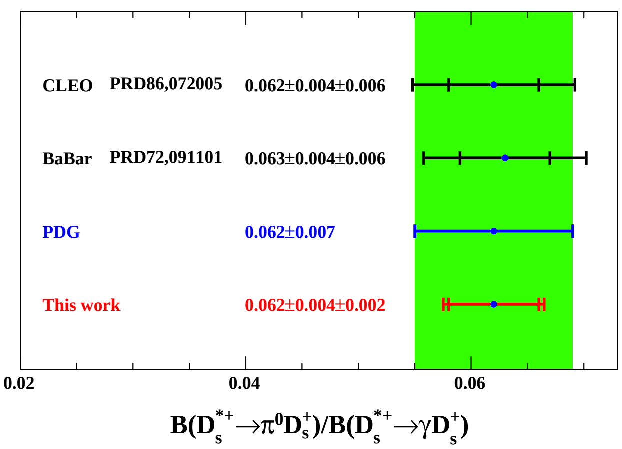

Fig. 3. Comparison of $\mathcal{B}_{D_s^{*+}\to D_s^+\pi^0}/\mathcal{B}_{D_s^{*+}\to D_s^+\gamma}$ measured by this work and previous experiments. The points with error bars are from different experiments. For each experiment, the shorter error bar denotes statistical only while the longer error bar combines both statistical and systematic uncertainties. The green band corresponds to the $\pm 1\sigma$ limit of the world average.

ACKNOWLEDGEMENTS

The BESIII collaboration thanks the staff of BEPCII and the IHEP computing center for their strong support. This work is supported in part by National Key R&D Program of China under Contracts Nos. 2020YFA0406400, 2020YFA0406300; National Natural Science Foundation of China (NSFC) under Contracts Nos. 11635010, 11735014, 11835012, 11935015, 11935016, 11935018, 11961141012, 12022510, 12025502, 12035009, 12035013, 12192260, 12192261, 12192262, 12192263, 12192264, 12192265; the Chinese Academy of Sciences (CAS) Large-Scale Scientific Facility Program; Joint Large-Scale Scientific Facility Funds of the NSFC and CAS under Contract No. U1832207, U1932102; 100 Talents Program of CAS; The Institute of Nuclear and Particle Physics (INPAC) and Shanghai Key Laboratory for Particle Physics and Cosmology; ERC under Contract No. 758462; European Union's Horizon 2020 research and innovation programme under Marie Sklodowska-Curie grant agreement under Contract No. 894790; German Research Foundation DFG under Contracts Nos. 443159800, Collaborative Research Center CRC 1044, GRK 2149; Istituto Nazionale di Fisica Nucleare, Italy; Ministry of Development of Turkey under Contract No. DPT2006K-120470; National Science and Technology fund; National Science Research and Innovation Fund (NSRF) via the Program Management Unit for Human Resources & Institutional Development, Research and Innovation under Contract No. B16F640076; STFC (United Kingdom); Suranaree University of Technology (SUT), Thailand Science Research and Innovation (TSRI), and National Science Research and Innovation Fund (NSRF) under Contract No. 160355; The Royal Society, UK under Contracts Nos. DH140054, DH160214; The Swedish Research Council; U. S. Department of Energy under Contract No. DE-FG02-05ER41374.

[1] H. Fritzsch, M. Gell Mann and H. Leutwyler, Phys. Lett. B **47**, 365 (1973).

[2] H. Y. Cheng, C. Y. Cheung, G. L. Lin, Y. C. Lin, T. M Yan and H. L. Yu, Phys. Rev. D **49**, 5857 (1994),

Table 4. Comparisons of the partial widths (Γ) and BFs (in brackets). The decay widths are in units of keV. The first two rows are from this work and the PDG, while the others are from various theoretical predictions. The superscript ^{a} denotes the value corresponding to $g = 0.52$, $\beta = 2.6$ GeV^{-1}, and $m_c = 1.6$ GeV; ^{b} denotes the values for a linear model; ^{c} denotes the value for $\kappa^q = 0.55$; and ^{d} denotes the values for (a) model.

	$\Gamma\,[\mathcal{B}]_{D_s^*\to D_s^+\gamma}$	$\Gamma\,[\mathcal{B}]_{D_s^*\to D_s^+\pi^0}$	$\mathcal{B}_{D_s^{*+}\to D_s^+\pi^0}/\mathcal{B}_{D_s^{*+}\to D_s^+\gamma}$
This work	...$[(93.57\pm0.41\pm0.16)\%]$	...$[(5.76\pm0.39\pm0.16)\%]$	$(6.16\pm0.40\pm0.17)\%$
PDG [17]	...$[(94.2\pm0.7)\%]$	...$[(5.9\pm0.7)\%]$	$(6.2\pm0.8)\%$
CM [14]	3.53 $[(92.7\pm0.7)\%]$	$0.277^{+0.028}_{-0.026}$ $[(7.3\pm0.7)\%]$	$(7.9\pm0.8)\%$
χPT [2][a]	4.5	...	...
χPT [3]	...	...	$8\times10^{-5}/\mathcal{B}(D^{*+}\to D^+\gamma)$
χPT [4]	0.32 ± 0.30	...	...
χPT [5]	...	$0.0081^{+0.0030}_{-0.0026}$	...
LFQM [6][b]	0.18 ± 0.01	...	...
RQM [7][c]	$0.321^{+0.009}_{-0.008}$	...	...
QCDSR [8]	0.25 ± 0.08	...	...
QCDSR [9]	0.59 ± 0.15	...	...
NJLM [10]	0.09	...	...
LQCD [11]	0.066 ± 0.026	...	...
NRQM [12]	0.21	...	...
NRQM [13][d]	0.40	...	...

Phys. Rev. D **55**, 5851(E) (1997).

[3] P. Cho and M. B. Wise, Phys. Rev. D **49**, 6228 (1994).

[4] B. Wang, B. Yang, L. Meng and S. L. Zhu, Phys. Rev. D **100**, 016019 (2019).

[5] B. Yang, B. Wang, L. Meng and S. L. Zhu, Phys. Rev. D **101**, 054019 (2020).

[6] H. M. Choi, J. Korean Phys. Soc. **53**, 1205 (2008).

[7] J. L. Goity and W. Roberts, Phys. Rev. D **64**, 094007 (2001).

[8] T. M. Aliev, E. Iltan and N. K. Pak, Phys. Lett. B **334**, 169 (1994).

[9] G. L. Yu, Z. Y. Li and Z. G. Wang, Eur. Phys. J. C **75**, 243 (2015).

[10] H. B. Deng, X. L. Chen and W. Z. Deng, Chin. Phys. C **38**, 013103 (2014).

[11] G. C. Donald, C. T. H. Davies, J. Koponen and G. P. Lepage, Phys. Rev. Lett. **112**, 212002 (2014).

[12] A. N. Kamal and Q. P. Xu, Phys. Lett. B **284**, 421 (1992).

[13] A. Fayyazuddin and O. H. Mobarek, Phys. Rev. D **48**, 1220 (1993).

[14] C. Y. Cheung and C. W. Hwang, Eur. Phys. J. C **76**, 19 (2016).

[15] J. Gronberg *et al.* (CLEO Collaboration), Phys. Rev. Lett. **75**, 3232 (1995).

[16] B. Aubert *et al.* (BaBar Collaboration), Phys. Rev. D **72**, 091101 (2005).

[17] P. A. Zyla *et al.* (Particle Data Group), Prog. Theor. Exp. Phys. **2022**, 083C01 (2022).

[18] M. Ablikim *et al.* (BESIII Collaboration), Nucl. Instrum. Meth. A **614**, 345 (2010).

[19] C. H. Yu *et al.*, Proceedings of IPAC2016, Busan, Korea, 2016, doi:10.18429/JACoW-IPAC2016-TUYA01.

[20] M. Ablikim *et al.* (BESIII Collaboration), Chin. Phys. C **44**, 040001 (2020).

[21] K. X. Huang *et al.*, Nucl. Sci. Tech. **33**, 142 (2022).

[22] X. Li *et al.*, Radiat. Detect. Technol. Methods **1**, 13 (2017); Y. X. Guo *et al.*, Radiat. Detect. Technol. Methods **1**, 15 (2017); P. Cao *et al.*, Nucl. Instrum. Meth. A **953**, 163053 (2020).

[23] M. Ablikim *et al.* (BESIII Collaboration), Chin. Phys. C **39**, 093001 (2015); Chin. Phys. C **46**, 113002 (2022). These articles described the integrated luminosity measurement for data taken at $\sqrt{s} = 4.189, 4.199, 4.209, 4.219$, and 4.226 GeV. The integrated luminosity values for the other data samples have been obtained by a similar procedure.

[24] S. Agostinelli *et al.* (GEANT4 Collaboration), Nucl. Instrum. Meth. A **506**, 250 (2003).

[25] S. Jadach, B. F. L. Ward and Z. Was, Phys. Rev. D **63**, 113009 (2001); Comput. Phys. Commun. **130**, 260 (2000).

[26] R. G. Ping, Chin. Phys. C **38**, 083001 (2014).

[27] D. J. Lange, Nucl. Instrum. Meth. A **462**, 152 (2001); R. G. Ping, Chin. Phys. C **32**, 599 (2008).

[28] J. C. Chen, G. S. Huang, X. R. Qi, D. H. Zhang and Y. S. Zhu, Phys. Rev. D **62**, 034003 (2000); R. L. Yang, R. G. Ping and H. Chen, Chin. Phys. Lett. **31**, 061301 (2014).

[29] E. Richter-Was, Phys. Lett. B **303**, 163 (1993).

[30] M. Ablikim *et al.* (BESIII Collaboration), Measuurement of the cross section for $e^+e^-\to D_s^{*\pm}D_s^{\mp}$ up to 4.7 GeV (to be published).

[31] M. Ablikim *et al.* (BESIII Collaboration), Phys. Rev. D **91**, 031101 (2015).